Moving particle simulation for a simplified permeability model of pervious concrete

Zilola Kamalova[a] and Shigemitsu Hatanaka[*]

Division of Architecture, Graduate School of Engineering, Mie University, Kurimamachiya-cho, Tsu, Mie, 514-8507, Japan

Abstract.   This study aimed to investigate the permeable nature of pervious concretes (PC) through the moving particle simulation (MPS) method. In the simulation, the complex structure of a pervious concrete was virtually demonstrated as a lattice model (LM) of spherical beads, where the test of permeability was conducted. Results of the simulation were compared with the experimental ones for validation. As a result, MPS results showed the permeability index of the LM as almost twice as big as the actual PCs. A proposed virtual model was created to prevent the stuck of water flow in the MPS simulation of PC or LM. Successful simulation results were demonstrated with the model.

Keywords: computer modeling; pervious concrete; concrete technology; construction materials; environmental effect; high/ultra-high performance concrete

1. Introduction

Pervious concrete (PC), alternatively known as porous concrete, is a type of concrete of coarse aggregates and a binding material that is characterized by a continuous void structure (Chindaprasirt *et al.* 2008, 2009, Hatanaka *et al.* 2012, 2014, Sata *et al.* 2016, Zhang *et al.* 2018, Zhu *et al.* 2018, Bu *et al.* 2018, Shatarat *et al.* 2018, Toghroli *et al.* 2018, Li *et al.* 2019). The desired void ratio (porosity) for PC is normally achieved with the addition of a small amount of fine aggregates, i.e., sand, to the binding material. In particular, PC void ratio typically ranges from 15% to 30%, with associated permeability of 1.4 to 12.4 mm/s (ACI 2010). With the large void structure as the main feature, PC pavements are permeable and potentially retain water, especially in urban areas, where such pavements allow rainwater to penetrate through their surfaces and reach the ground. Additionally, during heavy rains PC pavements contribute to the delay of water discharge from the city into the river, which makes them a specific interest as a countermeasure against floods caused by torrential rains. On the contrary, there are many uncertainties concerning the permeable nature of PCs.

PC permeability is commonly assessed using Darcy's law (Liu *et al.* 2018, Valeri *et al.* 2018, Mayorga *et al.* 2018), although several studies (Coleri *et al.*2013, Nielsen *et al.* 2007, Liu *et al.* 2018, Seoul Metropolitan City 2018) have argued the validity of its applicability for laminar flow through fine-grained sediments, i.e., soils, to evaluate the permeability characteristics of highly pervious coarse-grained materials. Asano *et al.* (2009) and Zhang *et al.* (2018) showed in experiments on PC mixtures that water flow inside a PC is a turbulent flow, which is well represented by Eq. (1a). Accordingly, this study adopted the nonlinear permeability formula in Eq. (1b), as proposed in the author's current work (Sekimoto 2017) for PC permeability assessment.

$$v = k' \cdot i^{m} \tag{1a}$$

$$v = k'_{(m=0.5)} \cdot i^{0.5} \tag{1b}$$

where v is the average flow velocity (cm/s), m is the power index, $k'_{(m=0.5)}$ is the nonlinear permeability index when $m=0.5$ (cm/s), and i is the hydraulic gradient.

Natsume *et al.* (2015), Hatanaka *et al.* (2015, 2019), and Matsuoka *et al.* (2016) used their test results to formulate Eq. (2) for determining the nonlinear permeability index $k'_{(m=0.5)}$ of PC as follows

$$k'_{(m=0.5)} = a \cdot V_R - b$$
$$a = 0.0083\varphi a + 0.042,$$
$$b = 0.11\varphi a + 0.54, \tag{2}$$

where V_R is void ratio (porosity) (%), and φa is the average diameter of aggregates (mm).

Due to the associated complexity in carrying out experimental designs for large-scale PC pavements, the use of simulations via computer technologies for solving problems relative to the utilization of PC is deemed much more economical and efficient. Thus, the authors herein aimed to apply the moving particle simulation (MPS) method to study water flow behavior inside a PC. MPS is specifically designed for incompressible fluids, as suggested by Koshizuka and Oka (1996), governed by continuity equations (Eq. (3)) and Navier–Stokes equation (Eq. (4)) as

*Corresponding author, Professor
  E-mail: hatanaka@arch.mie-u.ac.jp
[a]Former Graduate Student
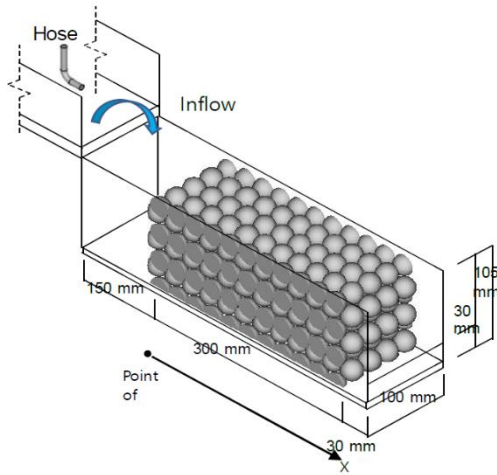 E-mail: lolalova13@gmail.com

Fig. 1 Dimensions of experimental model

where u, p, f, v, and ρ are the velocity, pressure, external force vector, kinematic viscosity, density of the fluid.

MPS has been popularly used in a wide range of research fields as for tsunami, flood, nozzle jet, and stirring of highly viscous liquids (Promotech Software 2018). Nonetheless, there has been no recorded account of its application for studying the permeability behavior of PCs.

The present study demonstrates such feasibility through simulations, in particular, using the software Particleworks, Ver.5.2.2 (Promotech Software 2018). Because the geometry of an actual PC is complex and difficult to reproduce with the software, it was simplified into a lattice model (LM) of spheres. The simulation results are validated through comparison with the experimental ones. For the experiment, the LM is fabricated using Styrofoam spherical beads. Moreover, both simulation and experimental results are analyzed to assess the horizontal permeability performance of the PC.

$$\frac{D\rho}{Dt} = 0 \tag{3}$$

$$\frac{Du}{Dt} = -\frac{\nabla P}{\rho} + v\nabla^2 u + f \tag{4}$$

2. Experiment

2.1 Outline of experiment

(a) D10-26%

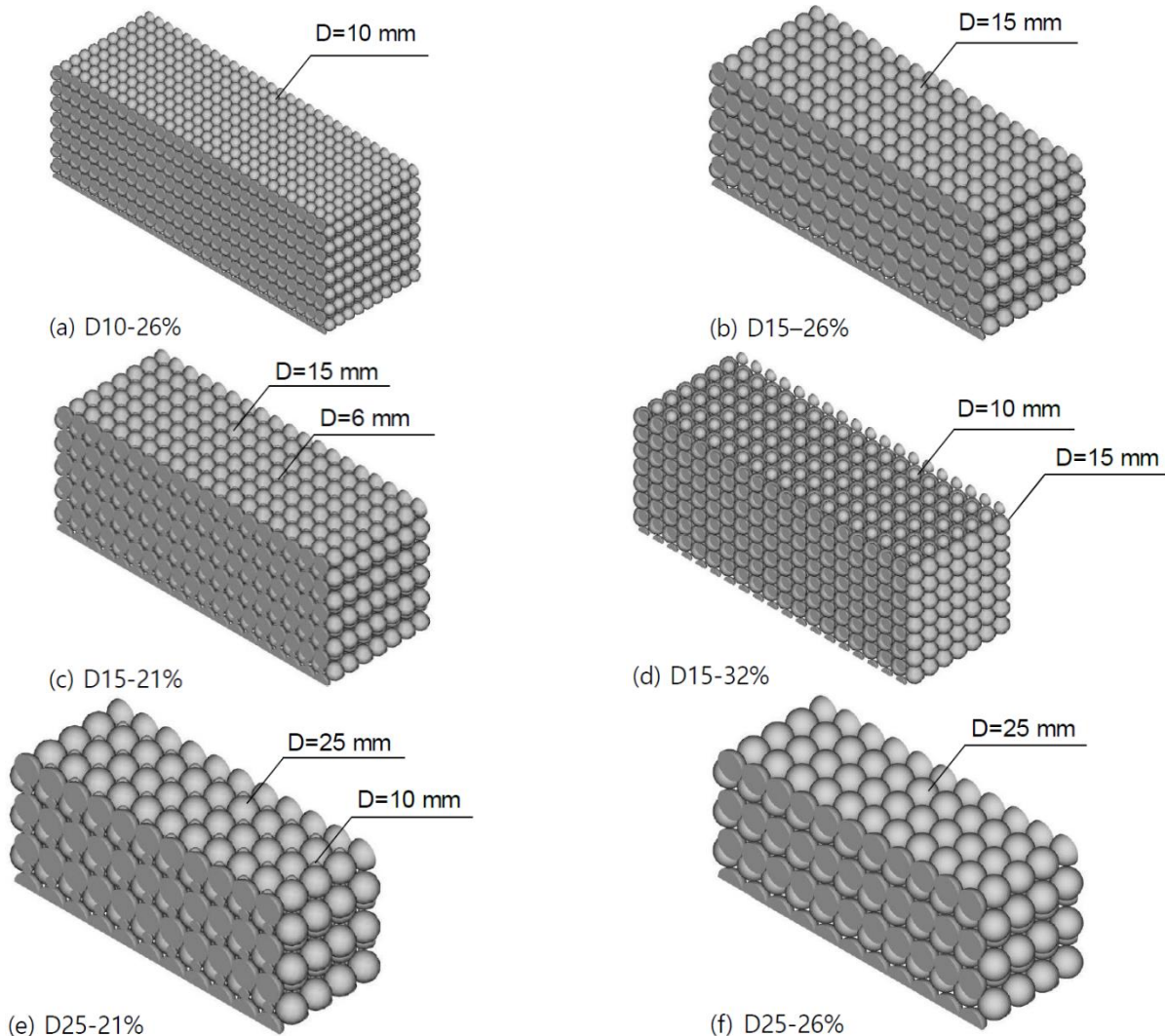(b) D15–26%

(c) D15-21%

(d) D15-32%

(e) D25-21%

(f) D25-26%

Fig. 2 Illustration of lattice models of 6 patterns (Name of model: Diameter-Void ratio)

Table 1 Factors and testing levels

Factor	Level
Material	foamed styrol
Diameter of bead (mm)	10. 15. 25
Void ratio (%)	21. 26. 32

Table 2 Illustration of unit grids of lattice models
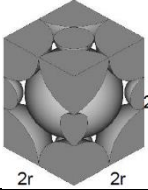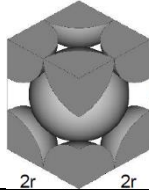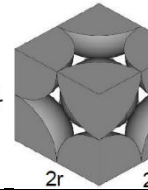
Void ratio (%)	21	26	32
Grid			

Photo 1 Side view of experimental layout

Fig. 1 illustrates the experimental setup, and Table 1 provides a list of all experimental factors and testing levels used. The LM specimen was made of Styrofoam beads with 10, 15, 25 mm of diameter and arranged in a body-centered cubic structure (see Fig. 2). Hemisphere beads were arranged along the walls of the formwork to avoid an increase in void ratio along walls (wall-effect) (Matsuoka 2016). The specimen was named according to its bead size and void ratio. The void ratio V_R of the models was set to 21%, 26%, and 32%, which is similar to the void ratio of widely used PC. Table 2 shows the unit grid of the LM, corresponding to each void ratio. Note that the grid is anisotropic in the case of V_R=21% and 26%. On average, the model dimensions were 300×100×105 mm (length, width, height; see Fig. 1). The height of the inflow was adjusted by arranging the location of a hose. A 30 mm high weir was set in the drainage side.

2.2 Experimental method

Photo 1 describes the actual conduct of the experiment. Here loads were placed on top of the model to restrain it from floating. Water level in the pouring surface was kept constant at 100 mm, and the amount of discharged water was measured for 10 s. Measurements were repeated 10 times. Water surface inside the model was also measured for calculations on hydraulic gradient (as explained below).

2.3 Experimental results

Eq. (5) was formulated based on Dupuit assumption (Yamaguchi 1984, Matsuoka 1984), for estimating the value of hydraulic gradient i. The hydraulic gradient was
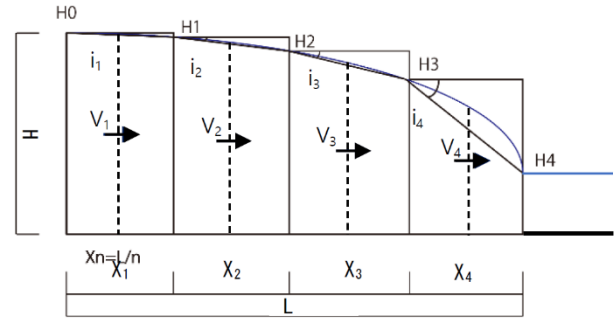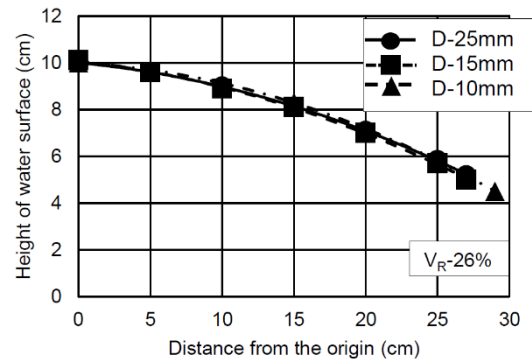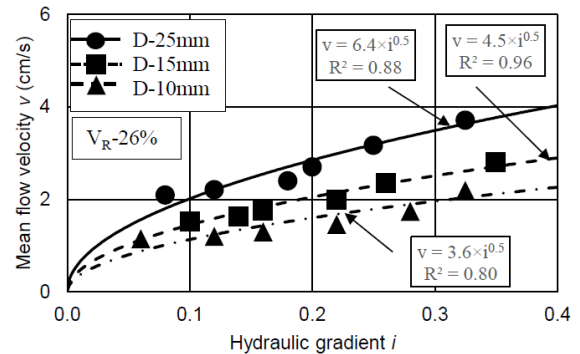
Fig. 3 Definition of hydraulic gradient in the horizontal direction

(a) Height of water surface in the horizontal axis

(b) Average flow velocity vs. hydraulic gradient

Fig. 4 Comparison of experimental results for D=10, 15, 25 mm and V_R=26%

calculated by dividing the water surface difference of the points $(H_{n-1} - H_n)$ by the distance between them X_n (see Fig. 3)

$$i_n=(H_{n-1}-H_n)/X_n, \qquad (5)$$

where i_n represents the nth hydraulic gradient, H_n the nth wet surface level (cm), and X_n the distance between the points (cm).

Accordingly, Eq. (6) was employed for estimating the mean flow velocity. Note that the actual flow velocity of water is given by $(v_n/V_R)\times100$, e.g., the actual value is $4v_n$ when V_R=25%.

$$v_n=Q / A_n \qquad (6)$$

where v_n is the mean flow velocity (cm/s), Q is the flow rate (cm³/s), and A_n is the section area of specimen (cm²).

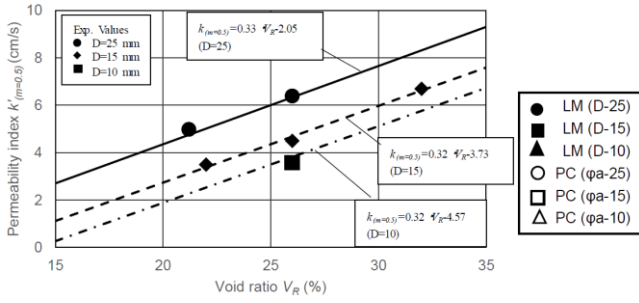The permeability index $k'_{(m=0.5)}$ was obtained from the

Fig. 5 Permeability index vs. void ratio

Table 3 Permeability indices of LM and PC

D (mm)	V_R (%)	$k'_{(LM)}$ (cm/s)	$k'_{(PC)}$ (cm/s)	α
10	26	3.6	1.6	2.2
15	21	3.5	1.5	2.4
	26	4.5	2.1	2.1
	32	6.7	3.1	2.1
25	21	5.0	2.0	2.5
	26	6.4	3.2	2.0

relationships of i_n and v_n following Eq. (1b). As an example, Fig. 4 shows the experimental results in case of the same void ratio but varying bead size ($D=2r$). Fig. 4(a) shows the height of water surface inside the model, whereas Fig. 4(b) shows the relationship between mean flow velocity and hydraulic gradient. Here, same height of water surface level (Fig. 4(a)), but varying permeability indices (Fig. 4(b)), were observed for all models, as a result of the different measured values for Q or v_n (Eq. (6)).

Fig. 5 illustrates the values of permeability index k' for all models (6 patterns). As for the tested void ratio, its linearity with the permeability index was observed, probably due to the same geometry of the grid. Such relationship is expressed in Eq. (7) (see Table 3 for the values of permeability indices), similarly as in the form of Eq. (2) for the actual PC

$$k'_{(m=0.5)} = c \cdot V_R + d$$
$$c = 0.00013D + 0.32$$
$$d = 0.17D - 6.25 \tag{7}$$

where V_R is void ratio (%), and D is diameter of the bead (mm).

2.4 Comparison of actual PC and LM

Table 3 and Fig. 6 provide a comparison of the values k' obtained for the actual PC (Eq. (2)) and LM (Eq. (7)). Here, coefficient α was introduced for evaluating the permeability of LM relative to that of actual PC, as in Eq. (8)

$$\alpha = k'_{(LM)}/k'_{(PC)} \tag{8}$$

where $k'_{(LM)}$ and $k'_{(PC)}$ represent the nonlinear permeability indices of LM and actual PC (both in cm/s), respectively.

Here, the average value of α was approximately 2.2, which indicates that the flow inside LM was 2.2 times faster, on average than that inside the actual PC, probably due to the difference in void geometry. Specifically, voids
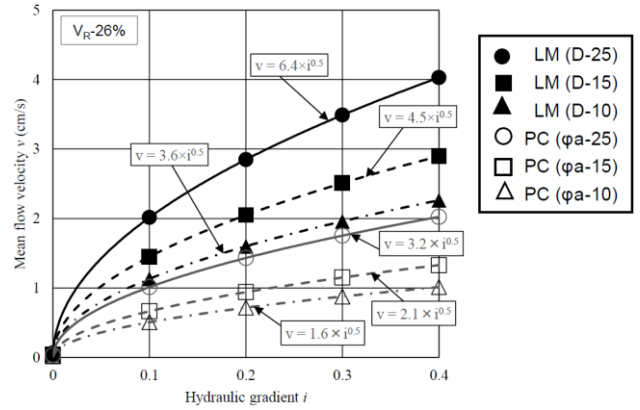

Fig. 6 Permeability indices $k'_{(LM)}$ and $k'_{(PC)}$ obtained from the average flow velocity-hydraulic gradient relation
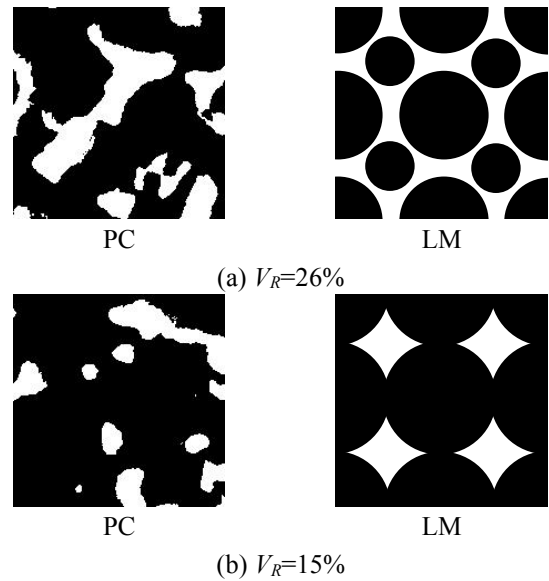

(a) V_R=26%

(b) V_R=15%

Fig. 7 Comparison of PC and LM sections (φa=16.5 mm for PC; D=15 mm for LM)

(a) Exaperiment
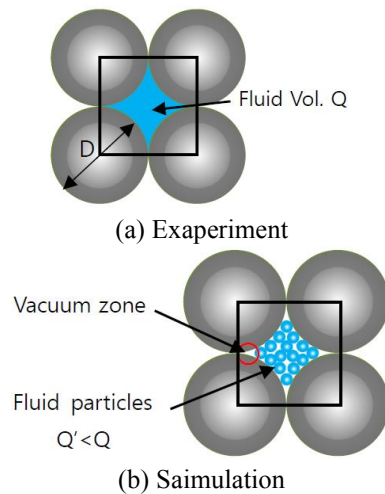

(b) Saimulation

Fig. 8 State of fluid flow

existed randomly in the actual PC, whereas those in LM took a uniformly consecutive form.

Furthermore, such difference in the values of α for LM
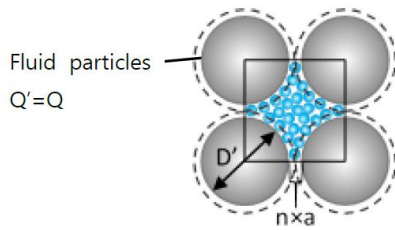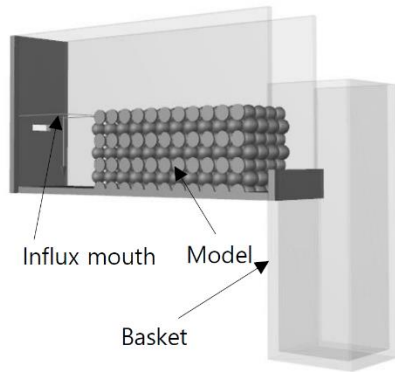
Fig. 9 Virtual model

Fig. 10 Simulation model (D25-26%)

Table 4 Simulation factors and levels

Factor	Level
Diameter of bead D (mm)	25
Void ratio V_R (%)	26
Initial distance between particles a (mm)	3
Multiplying factor n	0, 0.8, 0.9, 1, 1.15, 1.2, 1.25, 1.5

and the actual PC was considered as the main reason why water flow was apt to be more turbulent in the latter. Note that the coefficient α exhibited the tendency to rise with smaller void ratio. Fig. 7 typifies a comparison of PC and LM sections at almost the same void ratio. Here, it may be inferred that the void channels in the actual PC with 15% void ratio were not only narrower but also less connected, as compared to those of the PC with 26% void ratio.

3. MPS method

3.1 Construction of virtual model

During the simulation, the larger size of the fluid particle than actual water yields smaller flow rate than that in the experiment. Fig. 8 describes the state of flow inside the sectional area of the fluid. Note the formation of vacuum zones in Fig. 8(b) when the gap between the solid spheres was smaller than the fluid particle size.

The amount of water flow roughly equal to the experimental one was calculated by setting the size of the fluid particle (initial interparticle distance in MPS) to be sufficiently small for passage between the solid spheres. However, the memory capacity of the computer imposes limit on the size of the particle. Thus, it was deemed more beneficial to set large values to reduce the simulation

(a) View from the above
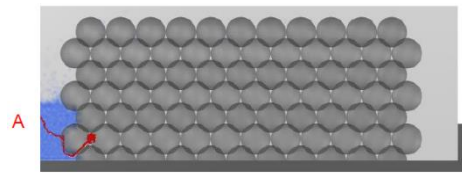
(b) View from the side

Fig. 11 Example of fluid particle flow behavior when n=0 (Simulation time, t=0−20s)

period. For this reason, the suggested approach was to minimize the size of the solid spheres without changing the grid (virtual model), as illustrated in Fig. 9. Here, the diameter of the solid sphere was reduced to a certain value, which ensures that the volume of fluid particles passing through the sectional area is equal to the experimental value.

Correspondingly, Eq. (9) was formulated for determining the proper value of the virtual solid sphere diameter as

$$D'=D-n\cdot a \qquad (9)$$

where D' and D denote the spherical diameters (mm) of the virtual and experimental models, n is the multiplying factor, and a is the initial inter-particle distance (mm).

3.2 Simulation model

A wide range of simulations was conducted for the same model (e.g., D25–26%, see Fig. 10) for the purpose of constructing a virtual LM. In the analysis, a hose was set as an inlet, and a box was installed on the drainage side to measure the flow rate. The dimensions of the models were set according to experimental model.

A preliminary simulation was conducted on the effect of initial inter-particle distance a, using a simulation model depicted in Fig. 10. The value of a was set to 1.5, 2, and 3 mm. After the simulation, the value of a was found to have no influence on the permeability index k' for a virtual LM, unless water particles are blocked and cannot move any more.

3.3 Simulation for determining n in Eq. (9)

Table 4 presents the simulation factors and levels. The value of n was set at 0 to 1.5, whereas the initial inter-particle distance was set to 3 mm, which causes the stuck of flow.

3.4 Simulation results

Table 5 shows the diameter sizes D' of the virtual models and the corresponding values of flow rate Q' and nonlinear permeability index k'. As mentioned above, when

Table 5 Values of *Q'* and *k'* for each multiplying factor *n* (*D*=25 mm, *a*=3 mm)

n	*D'* (mm)	Flow rate (cm³/s)	$k'_{(m=0.5)}$ (cm/s)
0	25	0	0.0
0.8	22.6	74	2.4
0.9	22.3	93	3.4
1	22	117	4.0
1.15	21.55	209	6.1
1.2	21.4	217	7.0
1.25	21.25	242	10.7
1.5	20.5	258	15.7
Ex. Value		205	6.4
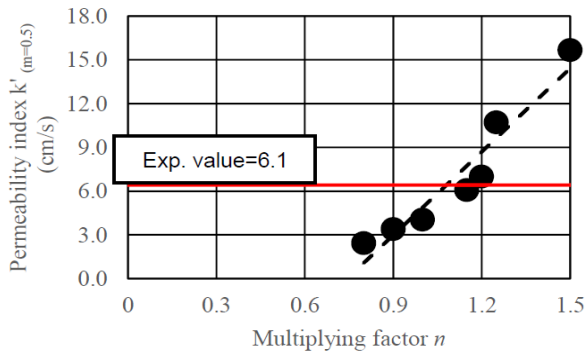
Fig. 12 Permeability index *k'* vs. multiplying factor *n*

(a) View from the above

― Trajectory of particle A

(b) View from the side

Fig. 13 A typical fluid particle flow behavior at *n*=1.15 (simulation time: *t*=0–20 s)
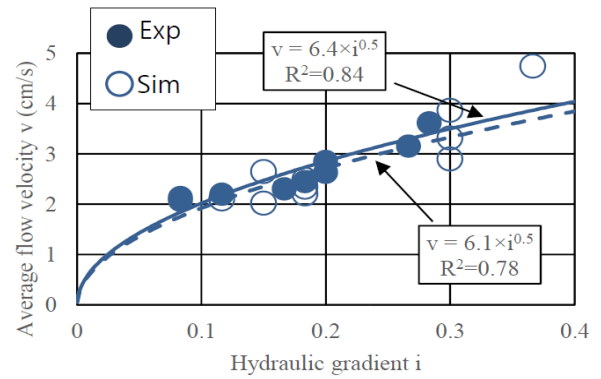
Fig. 14 Simulation and experimental values at *n*=1.15, D25-26%

n is 0, the fluid particles are entrapped and unable to pass through the medium (see Fig. 11). Fluid particles start to flow when *n*=0.8. Fig. 12 shows the relationship between *n* and *k'*. Here, note that *k'* was obtained from Eq. (1b), whereas *i* and *v* were obtained from Eqs. (5) and (6), respectively. *Q'* was obtained from Eq. (10)

$$Q' = N \cdot a^3 \qquad (10)$$

where *Q'* is the flow rate (mm³/s), *N* is the number of particles, and *a* is the initial inter-particle distance (mm) of the fluid particle.

The values of flow rate and permeability index were found to mostly match with the values of the experiment, when n is approximately 1.15, as recognized in Table 5, and as shown in flow state of fluid particles in Fig. 13. Figure 14 displays the comparison of the simulation and experimental values, which were found to be consistent with each other.

Table 6 shows the values of *k'* obtained from the horizontal permeability test, along with the corresponding
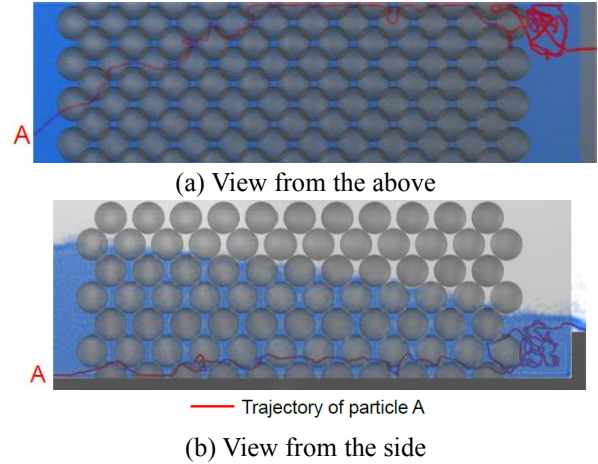
simulation results of all LMs used in this study. Moreover, the values of *n* ranged from 1.15 to 1.25.

The flow inside the model was further analyzed regarding turbulence. Fig. 15 shows the velocity distribution of fluid particles inside the model of D15%–22%. Here, the Reynolds number R_e calculated from Eq. (11) was governed by the particle moving velocity and varied from 9 to 4646, or an average value of 888. In Fig. 16, some fluid particles of different height at the initial stage (A, B, C) are traced. The Reynolds number and the tracing revealed that the turbulence of flow was successfully reproduced by the MPS method.

$$R_e = \frac{\rho_w D v}{\mu} \qquad (11)$$

Table 6 Values of multiplying factor *n* and simulation results

	Condition						Results		
Model	*D* (mm)	*d* (mm)	V_R (%)	*n*	*D'* (mm)	*d'* (mm)	$k'_{(Sim)}$ (cm/s)	$k'_{(Ex)}$ (cm/s)	$k'_{(Sim)}/k'_{(Ex)}$ (cm/s)
D10-26%	10	-	26	1.25	3.25	-	3.9	3.6	1.1
D15-21%		6	22	1.25	11.25	2.25	3.2	3.5	0.9
D15-26%	15	-	26	1.20	11.4	-	4.4	4.5	1.0
D10-32%		10	32	1.15	11.55	6.55	6.7	6.4	1.0
D25-21%	25	10	21	1.20	21.4	6.4	5.0	5.1	1.0
D25-26%		-	26	1.15	21.55	-	6.1	6.4	1.0
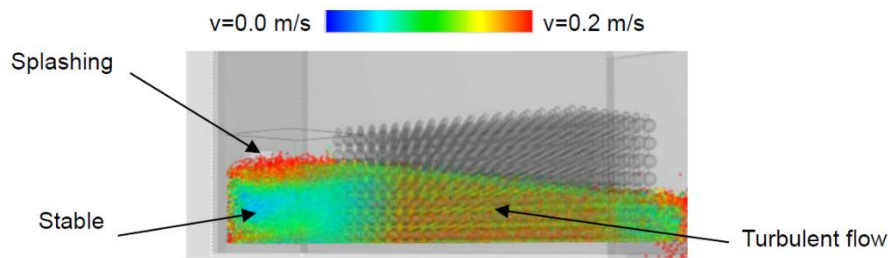
Fig. 15 Velocity distribution of fluid particles (D15-22%)
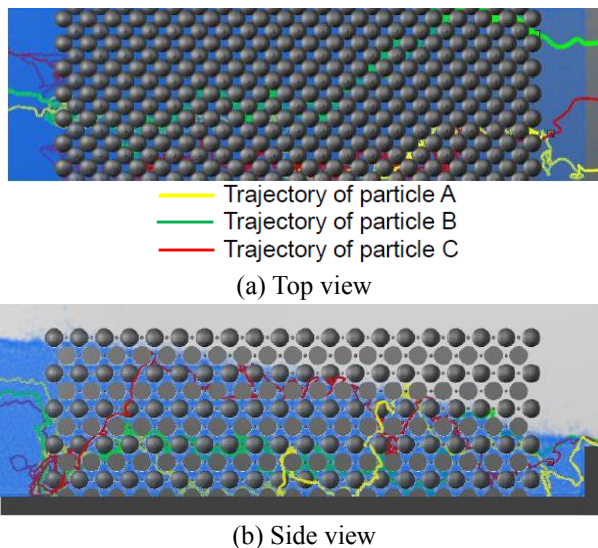

(a) Top view

(b) Side view

Fig. 16 A sample fluid particle trajectory (Simulation time, *t*=0–40s)

where ρ_w, D, v, and μ are the density of fluid, diameter of sphere, velocity of fluid, and dynamic viscosity of fluid, respectively.

4. Conclusions

This study centered on water flow behavior of various PCs via investigation through the MPS method. These findings could be generalized:

• The horizontal permeability test promotes the suitability of Eq. (7) to determine the nonlinear permeability index of a LM of arbitrary void ratio (porosity) and diameter size.

• A virtual model was fabricated for the MPS relative to inter-particle size restraints. Results of the simulations clarified the insignificant influence of inter-particle size on the permeability index of the virtual model, relative to the proposed Eq. (9) for diameter size determination.

• The experimental results, as well as MPS results showed the permeability index of LM as almost twice as big as the actual PCs.

• A proposed virtual model was created to avoid the entrapment of the fluid particles inside the medium. When the spherical diameter of the virtual model was reduced to 1.15 multiplied by the inter-particle distance, the simulation value for the permeability index matched with the experimental one.

References

ACI (2010), American Concrete Institute Committee 522, Report on Pervious Concrete, First Edition, American Concrete Institute, Michigan, USA, ACI 522R-10.

Asano, I., Hayashida, Y., Masukawa, S. and Tagashira, H. (2009), "Relationship between hydraulic gradient and discharge velocity in flow through pervious concrete", Technical Report of the National Institute for Rural Engineering, 227-241. (in Japanese)

Bu, J., Chen, X., Liu, S., Li, S. and Shen, N. (2018), "Experimental study on the dynamic behavior of pervious concrete for permeable pavement", *Comput. Concrete*, **22**(3), 291-303. https://doi.org/10.12989/cac.2018.22.3.291.

Chindaprasirt, P., Hatanaka, S., Chareerat, T., Mishima, N. and Yuasa, Y. (2008), "Cement paste characteristics and porous concrete properties", *Constr. Build. Mater.*, **22**, 894-901. https://doi.org/10.1016/j.conbuildmat.2006.12.007.

Chindaprasirt, P., Hatanaka, S., Mishima, N., Yuasa, Y. and Chareerat, T. (2009), "Effects of binder strength and aggregate size on the compressive strength and void ratio of porous concrete", *Int. J. Miner. Metal. Mater.*, **16**(6), 714-719. https://doi.org/10.1016/S1674-4799(10)60018-0.

Coleri, E., Kayhanian, M., Harvey, J.T., Yang, K. and Boone, J.M. (2013), "Clogging evaluation of open graded friction course pavements tested under rainfall and heavy vehicle simulators", *J. Environ. Manage.*, **129**, 164-172. https://doi.org/10.1016/j.jenvman.2013.07.005.

Hatanaka, S., Kamalova, Z. and Harada, M. (2019), "Construction of a nonlinear permeability model of pervious concrete and drainage simulation of heavy rain in a residential area", *Result. Mater.*, **3**, 100033. https://doi.org/10.1016/j.rinma.2019.100033.

Hatanaka, S., Mishima, N. and Natsume, M. (2015), "Study on

nonlinear coefficient of permeability of pervious concrete", *Proc. JPN Concrete Inst.*, **38**(1), 1381-1786. (in Japanese)

Hatanaka, S., Mishima, N., Maegawa, A. and Sakamoto, E. (2014), "Fundamental study on properties of small particle size porous concrete", *J. Adv. Concrete Technol.*, **12**(1), 24-33. https://doi.org/10.3151/jact.12.24.

Hatanaka, S., Mishima, N., Nakagawa, T., Morihana, H. and Chindaprasirt, P. (2012), "Finishing methods and compressive strength-void ratio relationships of in-situ porous concrete pavement", *Comput. Concrete*, **10**(3), 231-240. https://doi.org/10.12989/cac.2012.10.3.231.

Homepage of Promotech Software (2018), https://www.particleworks.com/case_study_ja.html.

Jiong, Z., Guodong, M., Ruiping, M., Xinzhuang, C., Li, L. and Huining, X. (2018), "Numerical study on seepage flow in pervious concrete based on 3D CT imaging", *Constr. Build. Mater.*, **161**, 468-478. https://doi.org/10.1016/j.conbuildmat.2017.11.149.

Koshizuka, S. and Oka, Y. (1996), "Moving-particle semi-implicit method for fragmentation of incompressible fluid", *Nucl. Sci. Eng.*, **123**, 421-434. https://doi.org/10.13182/NSE96-A24205.

Li, D., Toghroli, A., Shariati, M., Sajedi, F., Bui, D. T., Kianmehr, P., ... and Khorami, M. (2019) "Application of polymer, silica-fume and crushed rubber in the production of pervious concrete", *Smart Struct. Syst.*, **23**(2), 207-214. https://doi.org/10.12989/sss.2019.23.2.207.

Liu, H., Luo, G., Gong, Y. and Wei, H. (2018), "Mechanical properties, permeability, and freeze-thaw resistance of pervious concrete modified by waste crumb rubbers", *Appl. Sci.*, **8**(10), 1843. https://doi.org/10.3390/app8101843.

Liu, R., Liu, H., Sha, F., Yang, H., Zhang, Q., Shi, S. and Zheng, Z. (2018), "Investigation of the porosity distribution, permeability, and mechanical performance of pervious concretes", *Proc.*, **6**(7), 78. https://doi.org/10.3390/pr6070078.

Matsuoka, H. (1984), *Doshiturikigaku (Soil Mechanics)*, Morikitasyuppan, 32-53. (in Japanese)

Matsuoka, T., Sekimoto, R., Mishima, N. and Hatanaka, S. (2016), "Experimental study on influence of wall effect on nonlinear permeability behavior and its estimate of pervious concrete", *Proc. JPN Concrete Inst.*, **38**(1), 1749-1754. (in Japanese)

Mayorga, V.A.U., Garces, M.A.U., Gomez, D.P.P., Alvarado, Y.A., Torres, B. and Gasch, I. (2018), "Performance of pervious concrete containing combined recycled aggregates", *Ingenieria e Investigacion*, **38**, 34-41. http://dx.doi.org/10.15446/ing.investig.v38n2.67491.

Natsume, M., Mishima, N. and Hatanaka, S. (2015), "Experimental study on model of permeability of pervious concrete", *Proc. JPN Concrete Inst.*, **37**(1), 1375-1380. (in Japanese)

Nielsen, C.B. (2007), "Ravelling of porous pavements: assessment of test sections", Technical Note 48, Road Directorate, Danish Road Institute, Roskilde, Denmark.

Sata, V., Ngohpok, C. and Chindaprasirt, P. (2016), "Properties of pervious concrete containing high-calcium fly ash", *Comput. Concrete*, **17**(3), 337-351. https://doi.org/10.12989/cac.2016.17.3.337.

Sekimoto, R., Matsuoka, T., Mishima, N. and Hatanaka, S. (2017), "Modelling of nonlinear permeability behavior of porous concrete and drainage simulation of heavy rain in residential area", *Proc. JPN Concrete Inst.*, **39**(1), 1507-1512. (in Japanese)

Seoul Metropolitan City, Standard on Design, Construction, and Maintenance of Permeable Block Pavements, Ver. 2.0, 30. http://www.civiltech.co.kr/xe/66700.

Shatarat, N.K., Katkhuda, H.N., Hyari, K.H. and Asi, I. (2018), "Effect of using recycled coarse aggregate and recycled asphalt pavement on the properties of pervious concrete", *Struct. Eng.*

Mech., **67**(3), 283-290. https://doi.org/10.12989/sem.2018.67.3.283.

Toghroli, A., Shariati, M., Sajedi, F., Ibrahim, Z., Koting, S., Mohamad, E.T. and Khorami, M. (2018), "A review on pavement porous concrete using recycled waste materials", *Smart Struct. Syst.*, **22**(4), 433-440. https://doi.org/10.12989/sss.2018.22.4.433.

Valeri, V.C.A., Gandara, L.J., Espino, D.J. and Hernandez, J.R. (2018), "Characterization of the infiltration capacity of porous concrete pavements with low constant head permeability tests", *Molecul. Divers. Preserv. Int., Water*, **10**(4), 480. https://doi.org/10.3390/w10040480.

Yamaguchi, H. (1984), *Doshistu-rikigaku Zenkaitei (Total Revision of Soil Mechanics)*, Gihoudou-syuppan, 53-64. (in Japanese)

Zhang, W., Li, H. and Zhang, Y. (2018), "Effect of porosity on frost resistance of Portland cement pervious concrete", *Adv. Concrete Constr.*, **6**(4), 363. https://doi.org/10.12989/acc.2018.6.4.363.

Zhu, X., Chen, X., Shen, N., Tian, H., Fan, X. and Lu, J. (2018), "Mechanical properties of pervious concrete with recycled aggregate", *Comput. Concrete*, **21**(6), 623-635. https://doi.org/10.12989/cac.2018.21.6.623.

HK